REPORT DOCUMENTATION PAGE

Form Approved
OMB No. 0704-0188

1. REPORT DATE *(DD-MM-YYYY)*	**2. REPORT TYPE**	**3. DATES COVERED** *(From - To)*
Mar 2014	Journal Article	Mar 2014- Dec 2014

4. TITLE AND SUBTITLE

Formulation and Physical Properties of Cyanate Ester Nanocomposites Based on Graphene

5a. CONTRACT NUMBER
In-House

5b. GRANT NUMBER

5c. PROGRAM ELEMENT NUMBER

6. AUTHOR(S)
Josiah T. Reams, Andrew J. Guenthner, Kevin R. Lamison, Gregory R. Yandek, David D. Swanson, and Joseph M. Mabry

5d. PROJECT NUMBER

5e. TASK NUMBER

5f. WORK UNIT NUMBER
Q16J

7. PERFORMING ORGANIZATION NAME(S) AND ADDRESS(ES)

Air Force Research Laboratory (AFMC)
AFRL/RQRP
10 E. Saturn Blvd.
Edwards AFB, CA 93524-7680

8. PERFORMING ORGANIZATION REPORT NO.

9. SPONSORING / MONITORING AGENCY NAME(S) AND ADDRESS(ES)

Air Force Research Laboratory (AFMC)
AFRL/RQR
5 Pollux Dr.
Edwards AFB, CA, 93524-7048

10. SPONSOR/MONITOR'S ACRONYM(S)

11. SPONSOR/MONITOR'S REPORT NUMBER(S)
AFRL-RQ-ED-JA-2014-297

12. DISTRIBUTION / AVAILABILITY STATEMENT
Approved for public release; distribution unlimited

13. SUPPLEMENTARY NOTES
Journal article published in the Journal of Polymer Science Part B, Vol#52, Issue #16, 15 August 2014.
PA Case Number: #14557; Clearance Date: 20 Nov 2014.

14. ABSTRACT
We report the thermal, mechanical, and diffusion properties of bisphenol E based polycyanurate nanocomposites with three forms of graphene derived from sequential processing of the same carbon nanostructure. Edgefunctionalized graphene nanoplatelets (GNP) were converted to graphene oxide (GO), then heated to produce thermally reduced graphene oxide (TRGO). All three reinforcements were individually mixed with the dicyanate ester of bisphenol E (LECy) at low loading levels and cured to form polycyanurate nanocomposites. GNP, with very low oxygen functionality, was incompatible with the cyanate ester, while the highly oxidized GO formed well-dispersed (though not exfoliated) nanocomposites, with the TRGO forming a good dispersion on mixing but phase separating during cure. The addition of GO, and, to a lesser extent, TRGO, resulted in improved mechanical properties, particularly fracture toughness, with the addition of TRGO having a modestly negative effect on the glass transition temperature. Surprisingly, neither GO nor TRGO addition was effective at slowing down the diffusion of water in the polycyanurate, with the addition of both resulting in increased equilibrium moisture uptake. It thus appears that the trade-off between dispersion and the required level of oxygen functionality acts in a manner to frustrate attempts at minimizing the permeation of water by addition of graphene-based reinforcements.

15. SUBJECT TERMS

16. SECURITY CLASSIFICATION OF:			**17. LIMITATION OF ABSTRACT**	**18. NUMBER OF PAGES**	**19a. NAME OF RESPONSIBLE PERSON**
					Joseph Mabry
a. REPORT	**b. ABSTRACT**	**c. THIS PAGE**			**19b. TELEPHONE NO** *(include area code)*
Unclassified	**Unclassified**	**Unclassified**	SAR	11	661-275-5664

Standard Form 298 (Rev. 8-98)
Prescribed by ANSI Std. 239.18

Formulation and Physical Properties of Cyanate Ester Nanocomposites Based on Graphene

Josiah T. Reams,[1] Andrew J. Guenthner,[2] Kevin R. Lamison,[1] Gregory R. Yandek,[2] David D. Swanson,[2]* Joseph M. Mabry[2]

[1]ERC Incorporated, Air Force Research Laboratory, Edwards AFB, California 93524
[2]Air Force Research Laboratory, Aerospace Systems Directorate, Edwards AFB, California 93524
Correspondence to: J. T. Reams (E-mail: Josiah.reams.ctr@us.af.mil)

Received 6 March 2014; revised 15 May 2014; accepted 2 June 2014; published online 00 Month 2014
DOI: 10.1002/polb.23532

ABSTRACT: We report the thermal, mechanical, and diffusion properties of bisphenol E based polycyanurate nanocomposites with three forms of graphene derived from sequential processing of the same carbon nanostructure. Edge-functionalized graphene nanoplatelets (GNP) were converted to graphene oxide (GO), then heated to produce thermally reduced graphene oxide (TRGO). All three reinforcements were individually mixed with the dicyanate ester of bisphenol E (LECy) at low loading levels and cured to form polycyanurate nanocomposites. GNP, with very low oxygen functionality, was incompatible with the cyanate ester, while the highly oxidized GO formed well-dispersed (though not exfoliated) nanocomposites, with the TRGO forming a good dispersion on mixing but phase separating during cure. The addition of GO, and, to a lesser extent, TRGO, resulted in improved mechanical properties, particularly fracture toughness, with the addition of TRGO having a modestly negative effect on the glass transition temperature. Surprisingly, neither GO nor TRGO addition was effective at slowing down the diffusion of water in the polycyanurate, with the addition of both resulting in increased equilibrium moisture uptake. It thus appears that the trade-off between dispersion and the required level of oxygen functionality acts in a manner to frustrate attempts at minimizing the permeation of water by addition of graphene-based reinforcements. © 2014 Wiley Periodicals, Inc. J. Polym. Sci., Part B: Polym. Phys. **2014**, *00*, 000–000

KEYWORDS: composites; crosslinking; compatibility; nanocomposites; resins; toughness

INTRODUCTION Graphene, an allotrope of carbon, is an atomically thick monolayer of carbon atoms arranged in a honeycomb-like lattice. Interest in this material has grown rapidly in recent years due to its unusual properties. Graphene is the strongest material measured to date and can display exceptionally high thermal conductivity, electrical conductivity, and gas impermeability, making it a potential next generation nanomaterial for property improvement in polymer nanocomposite materials.[1–6] Unlike alternative allotropes of carbon (fullerenes, carbon nanotubes, and diamond) graphene can be isolated as individual sheets from relatively inexpensive graphite.[7–10]

The strong pi stacking of graphite has thus far prevented the direct dispersion of individual graphene sheets, or even multilayer graphene into polymer systems. Chemical oxidation of graphite to graphene oxide (GO) can be accomplished by treatment of graphite with strong oxidizing agents.[11–13] This chemical modification results in the incorporation of surface hydroxyl and epoxide groups, as well as carbonyl functionalities at the edges.[14,15] The oxygen functionalities of GO allow dispersion in polar solvents and many polymeric systems.[16,17] GO undergoes simultaneous reduction and exfoliation when heated rapidly above 550 °C.[18,19] The resulting thermally reduced graphene oxide (TRGO) has much lower oxygen content. However, due to the irregular shape of TRGO, it can still be dispersed in organic solvents with sonication.

GO and TRGO have been shown to impart physical and mechanical property improvements to both thermoplastic and thermosetting polymer systems.[17,20] Low loadings of TRGO in epoxy matrices results in composites with increased modulus, increased fracture toughness and lower water uptake over neat epoxy.[21–24] Increased fracture toughness was also observed for amine-functionalized GO in epoxy.[25] While the degree of property improvement versus loading level of graphene, compared to other carbon allotropes, has been investigated, little work has been reported on the

*Present address: David D. Swanson, Air Force Nuclear Weapons Center, Hill AFB, UT 84040

Additional Supporting Information may be found in the online version of this article.

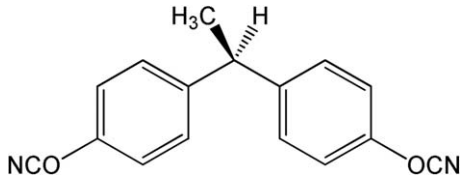

FIGURE 1 Chemical Structure of LECy.

property improvement of graphene with differing levels of oxidation on physical and mechanical properties.[24]

Cyanate ester resins are a class of thermosetting materials that are finding increasing uses due to their relatively low water uptake, strength at high temperatures and ease of processing. Monomers such as Primaset LECy (the dicyanate ester of bisphenol E) (Fig. 1), have melting points at or just above room temperature, making them suitable for applications such as filament winding and nanomolding.[26,27] Recent investigations of cyanate ester resins as high temperature materials for space and propulsion applications have brought attention to the need for high temperature composite materials with improved stiffness, strength, hot/wet performance and high maximum use temperatures.[28,29] Improvement in the stiffness and strength of cyanate esters has been achieved by blending with a thermoplastic polymer or addition of a nanosized filler.[30,31] Graphene has the potential to impart improvements not only in stiffness and strength but, because graphene is an excellent barrier, also has the potential to decrease water uptake and therefore increase hot/wet performance.

Lin et al. investigated the effect of isocyanate modified GO on the flexural strength, impact strength and thermal stability of a polycyanurate-bismaleimide system consisting of bisphenol A dicyanate (BADCy), 4,4′-bismaleimidodiphenyl methane and *o,o′*-diallylbisphenol A.[32] It was found that flexural strength, impact strength, and char yield increased for isocyanate modified GO up to 1 wt % loading. Wang et al. investigated the effect of GO on the cure kinetics of GO/PT-30 composites.[33] It was found that increasing amounts of GO decreased the peak exotherm temperatures, by 97 °C for 4 wt % GO, in dynamic DSC. Using the Kamal model, the activation energies (E1) corresponding to early stages of cure decreased with increasing GO content, while the late-stage cure activation energy (E2) decreased with up to 2 wt % GO then increased with 4 wt % GO to a value identical to pure PT-30. The effect of incorporation of GO or other forms of graphene on the critically important water uptake and hydrolytic stability properties of polycyanurate resins, however, has not been previously reported to our knowledge.

Three different forms of graphene were used in this study: M-25 graphite nanoplatelets (GNP) GO, and TRGO. The graphite nanoplatelets were dispersed in LECy polycyanurate, and used as a starting material for oxidation to form the GO. Some of the GO in turn was heated to form the thermally reduced GO. The use of these sequentially processed nanomaterials allows for investigation of the effect of graphene with a wide range of functionalization and surface area on polycyanurate properties while maintaining the maximum level of comparability between the nanoscale reinforcements.

For this study, we hypothesized that altering the degree of oxidation of graphene changes the interaction energy between the reinforcement and the matrix in graphene/cyanate ester composites, affecting dispersion and phase separation during cure, and thereby leading to differences in the microscale morphology of the cured composites. The differences in morphology in turn will influence key physical properties. In addition, altering the degree of graphene oxidation also changes the morphology of the graphene itself on the nanoscale, leading to further differences in dispersion, phase separation, and physical properties of the cured composites. Lastly, the addition of graphene to polycyanurate may alter network formation either through reaction of cyanate esters with surface functional groups or impurities introduced from the chemically oxidized graphite. Our results indicated that increased oxidation in GO and TRGO led to better dispersion (though not to intercalation or exfoliation) during mixing. The nanoscale morphology of TRGO, however, appeared to inhibit good dispersion by facilitating the formation of percolating nanoparticle networks. Although the well-dispersed GO retained a highly anisotropic particle shape (which should inhibit diffusion by increasing the tortuosity of permeation pathways), the highly favorable interaction between GO and intercalated water appeared to "short circuit" the diffusive barrier. Thus, improved moisture barrier performance was not attained in cyanate ester composites. These results therefore provide important new information for understanding the performance of graphene/polymer nanocomposites, while also demonstrating an elegant way of investigating the effects of variables such as surface polarity and particle morphology on the performance of graphene nanocomposites.

EXPERIMENTAL

Materials

The dicyanate ester of bisphenol E [Primaset® LECy, that is, 1,1-bis(4-cyanatophenyl)ethane], see Figure 1 for chemical structure, was purchased from Lonza and used as received. Nonylphenol (technical grade) was purchased from Aldrich, and Copper (II) acetylacetonate was purchased from ROC/RIC; both were used as received. Graphite nanoplatelets (xGNP-M-25) were purchased from XG Sciences® and have an average thickness of 6 nm and average diameter of 25 μm.

Batches of catalyst comprised of 30 parts by weight nonylphenol to one part by weight of copper (II) acetylacetonate were prepared by mixing the ingredients in a vial and heating to 60 °C while stirring vigorously until complete dissolution took place (typically 1–2 h). These batches were retained for up to 30 days.

GO was prepared from xGNP-M-25 graphite nanoplatelets by a modified Hummers oxidation method.[13] Graphite

nanoplatelets were chosen as a starting material over bulk graphite with the expectation that the small particle dimensions (6 nm thick × 25 μm lateral diameter, per the manufacturer) would yield GO with the greatest degree of oxidation possible under the oxidation conditions used. In a 2 L Erlenmeyer flask, 10 g of xGNP-M-25 graphite nanoplatelets were suspended in a solution of 230 mL of concentrated sulfuric acid and 5.0 g of sodium nitrate. The solution was cooled to 0 °C by placing the flask in an ice bath and 30 g of potassium permanganate was added slowly with stirring which caused the suspension to turn to a thick paste. After the addition of potassium permanganate the solution was warmed to 35 °C and allowed to stir for 30 min. After this time 460 mL of deionized water was added slowly, which caused the temperature of the suspension to rise to 98 °C. The temperature was held at 98 °C for 15 min. The suspension was then diluted to ~1.4 L with water and treated with 150 mL of a 3% hydrogen peroxide solution. The suspension was then filtered through a glass fritted funnel while warm and washed three times with a 5% hydrochloric acid solution, once with water and once with acetone. TRGO was prepared by placing 5.0 g of GO in a covered graphite boat which was heated in a tube furnace at 800 °C for 5 min with flowing nitrogen.

Composite Sample Preparation

Composite resins were fabricated by first mixing LECy with two parts per hundred by weight of catalyst and 1 wt % GO, TRGO or M-25 graphite. The mixture was then mixed with an IKA T25 Basic high shear mixer for 1 h followed by ultrasonication for 1 h. The mixture was partially de-gassed at 90 °C for 30 min under reduced pressure (300 mm Hg). To prepare cured samples for TMA, silicone molds made from R2364A silicone from Silpak (mixed at 10:1 by weight with R2364B platinum-based curing agent) were made by de-gassing for 60 min at 300 mm Hg, cured overnight at room temperature, followed by postcure at 150 °C for 1 h. The uncured cyanate ester mixture was then poured into the mold. The open mold and sample were then placed under flowing nitrogen at 25 °C and ramped 5 °C min^{-1} to 150 °C for 1 h, ramped 5 °C min^{-1} to 210 °C for 24 h to produce void-free discs measuring ~11.5–13.5 mm in diameter by 1–3 mm thick and weighing 200–400 mg. Composite samples for dynamic mechanical analysis (DMA) were made using the above procedure with open molds that gave rectangular samples measuring 60 × 13 × 2.5 mm^3.

Composite panels were fabricated by first mixing LECy with two parts per hundred by weight of catalyst and 1 wt % GO or TRGO. The mixture was then mixed with an IKA T25 Basic high shear mixer for 1 h followed by ultrasonication for 1 h. The mixture was partially degassed at 90 °C for 30 min under reduced pressure (300 mm Hg). After degassing, the mixture was immediately injected into a preheated (90 °C) flat-panel mold made of TEFLON® coated steel plates and a silicone spacer made from R2364A silicone from Silpak prepared in the same manner as the silicone used for TMA and DMA samples. The resin mixture was then cured under flowing nitrogen by the cure schedule described above. The resulting panels had dimensions of 7.6 × 7.6 × 0.32 cm^3. The panels were cut into 7.6 × 1.27 cm sections for flexural analysis and 2.54 × 1.27 cm sections for room temperature water diffusion measurements.

Characterization

DSC was performed on a TA Instruments Q2000 calorimeter under 50 mL min^{-1} of flowing nitrogen. The samples were heated to 350 °C, then cooled to 25 °C and reheated to 350 °C, all at 10 °C min^{-1}. Oscillatory TMA was conducted with a TA Instruments Q400 series analyzer under 50 mL min^{-1} of nitrogen flow. The discs were held in place via a 0.2 N initial compressive force with the standard ~5 mm diameter flat cylindrical probe while the probe force was modulated at 0.05 Hz over an amplitude of 0.1 N (with a mean compressive force of 0.1 N) and the temperature was ramped to 350 °C followed by two heating and cooling cycles between 100 and 200 °C (to determine thermal lag), and a final ramp to 350 all at 10 °C min^{-1} for the GO composite samples and 20 °C min^{-1} for the M-25 composite and for the neat LECy resin. The details of determining thermal lag can be found elsewhere.[28] Linear coefficients of thermal expansion (CTEs) were determined from the dimension change of the cylindrical sample with respect to temperature. All values are reported in ppm $°C^{-1}$ at 75 °C. DMA was performed with a TA Instruments Q800. Rectangular samples with typical dimensions 60 × 13 × 2.5 mm^3 were analyzed in dual cantilever mode and ramped at 5 °C min^{-1} from 25 to 350 °C at a frequency of 1 Hz and amplitude of 10 μm. Dispersions of GO in water were spin-cast on freshly cleaved mica for AFM imaging. AFM images were obtained using a Veeco Digital Instruments Nanoscope IV in tapping mode. SEM images of fractured surfaces were obtained with a FEI Quanta 600 SEM in high vacuum mode. Samples were gold sputtered (~1 nm thickness) prior to imaging. TEM imaging was performed by the University of Dayton Research Institute (UDRI) on a Hitachi H7600 run at 100 kV. Samples for TEM imaging were prepared on a Leica EM UC 6 ultramicrotome. The microtomed samples were then placed on holey carbon coating on 400 mesh copper grids. X-ray diffraction measurements were performed on a Bruker AXS D2 Phaser equipped with a LYNXEYE detector and CuKα source in the 2θ angle range of $5.0° - 35.0°$. Elemental analysis was performed by Atlantic Microlab. Ambient temperature (20 °C) water diffusion experiments were performed on rectangular samples with dimensions of 31 × 12 × 3 mm^3. Sample masses were measured at periodic intervals for 2500 h. The diffusion coefficient (D) was calculated using the equation:

$$D = \frac{\pi}{t}\left(\frac{lM_t}{4M_m}\right)^2 = \pi\left(\frac{l\theta}{4M_m}\right)^2$$

where Θ is the initial linear slope of the plot of the percent weight gain (M_t) versus $t^{1/2}$, which, for the samples investigated here, was from 0 to ~150 h.[34,35] The equilibrium weight gain (M_m) was estimated as the weight gain at $t = 2500$ h.

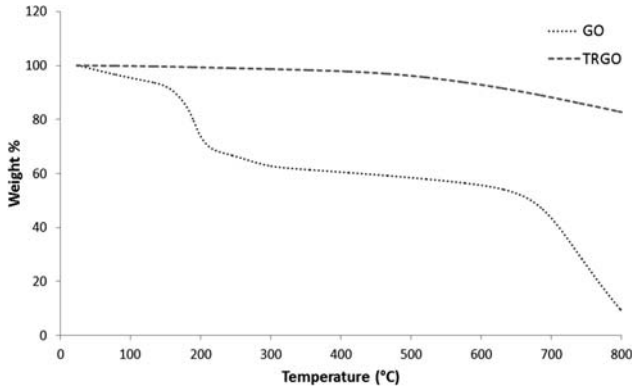

FIGURE 2 Weight loss versus temperature in nitrogen for GO and TRGO. [Color figure can be viewed in the online issue, which is available at wileyonlinelibrary.com.]

RESULTS AND DISCUSSION

Characterization of GO and TRGO Structure

The formation of GO was confirmed both by AFM imaging of single sheets exfoliated in water, as well as X-ray diffraction, which showed a major reflection at $2\Theta = 12.6^\circ$ (within the range of reported values for GO).[36–38] More details are provided in Supporting Information. Thermogravimetric analysis (TGA) of as-prepared GO showed three distinct weight loss regions (Fig. 2). These have been shown to arise from evaporation of intercalated water at 50–150 °C, loss of oxygen functional groups at 200 °C and sublimation of the carbon backbone at 700–800 °C.[18] The degree of oxidation of GO was quantified by the weight loss at 200 °C and was found to be ~30%, a figure confirmed by elemental analysis (Table 1).

Weight loss at 200 °C was absent from the TGA scan of TRGO, indicating that the thermal treatment of GO to produce TRGO resulted in nearly complete removal of at least some oxygen functionalities (Fig. 2). Furthermore, weight loss in the 50–150 °C region was absent in TRGO indicating that TRGO does not contain adsorbed water like GO. Significant, though not complete, loss of oxygen functionality was also confirmed by the C content obtained from elemental analysis of TRGO samples. Because oxygen-containing groups will contribute to the polarity of the graphene surfaces, in terms of polarity, the three types of graphene studied may be ordered in terms of decreasing surface polarity as GO > TRGO > untreated M-25.

TABLE 1 Oxygen Content from Elemental Analysis[a] and TGA[b]

Sample	Oxygen Content[a] (wt %)	Oxygen Content[b] (wt %)
GO	33.2 ± 0.3	31
TRGO	14.7[†]	1

[†] Oxygen content estimated from C and H combustion analysis.
[a] Oxygen content obtained by C, H, O combustion analysis unless otherwise noted.
[b] Oxygen content estimated from TGA weight loss.

Morphology of Graphene/Cyanate Ester Composites

TEM images of the untreated M-25 in a 1 wt % nanocomposite with LECy show that the nanoscale morphology of the M-25 GNP remains unaltered by incorporation into the LECy matrix and subsequent cure, with the M-25 GNP remaining as well-ordered stacks of graphene sheets with relatively well-aligned edges (see Supporting Information). TEM of the 1 wt % GO nanocomposites show that the GO is not fully exfoliated and is present as many-layered stacked sheets with stepped edges (Fig. 3, also see Supporting Information). These stepped edges result from restacking of the GO during drying after oxidation. In contrast, TRGO in the LECy composites is not stacked but is present in more loosely associated sheets that have a shredded and wrinkled morphology (Fig. 4, with additional examples in Supporting Information). The shredded and wrinkled nature of the sheets reflects the rapid expansion of intercalated water during thermal reduction. Thermal reduction thus causes both a decrease in surface polarity and a significant change in nanoscale morphology.

Although GO exists as stacked sheets, low magnification TEM shows the GO stacks exist as relatively isolated individual particles (an indication of good dispersion maintained throughout cure), while the TRGO "shredded stacks" tend to intermingle with one another to form co-continuous resin rich and TRGO rich regions on the micron scale (see Supporting Information). The alteration of morphology produced by thermal reduction of GO thus extends beyond the nanoscale to the micron scale, and is therefore expected to influence dispersion behavior.

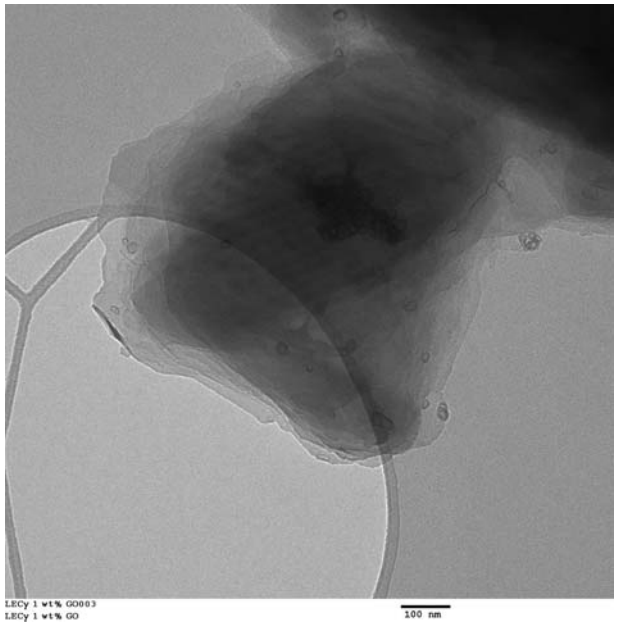

FIGURE 3 TEM image of 1 wt % GO LECy polycyanurate.

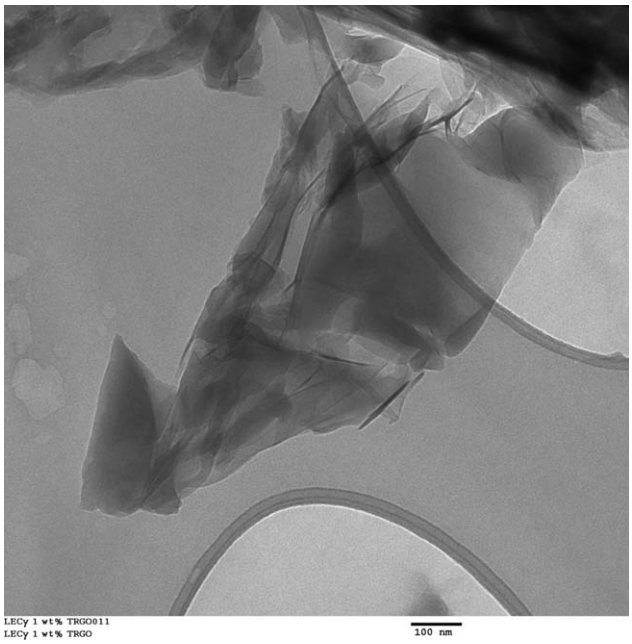

FIGURE 4 TEM image of 1 wt % TRGO LECy polycyanurate

To further investigate both the morphology and the interaction between GO and TRGO, and the polycyanurate matrix, SEM images of fractured surfaces of GO and TRGO composites were obtained. The surface topology of the polycyanurate samples in which GO and TRGO were dispersed displayed a characteristic roughness that was not present in the fracture surface of neat LECy polycyanurate (see Supporting Information). In the GO nanocomposite samples, areas of the fracture surface where GO sheets were found protruding from the surface were clearly observed (Fig. 5).

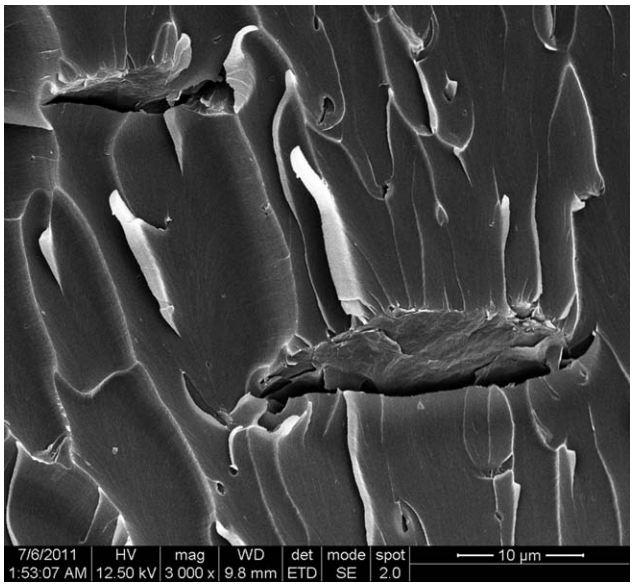

FIGURE 5 SEM image of the fractured surface of 1 wt % GO LECy polycyanurate.

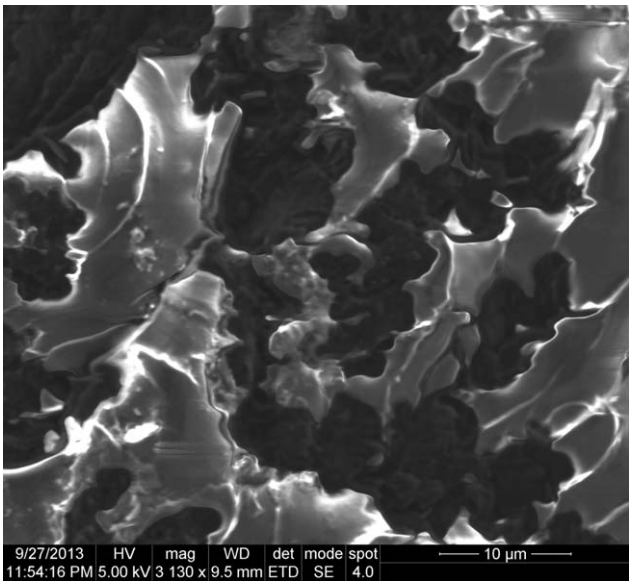

FIGURE 6 SEM image of the fractured surface of 1 wt % TRGO LECy polycyanurate.

Although good dispersion (meaning that individual stacks of GO sheets were relatively isolated from one another at the micron scale) was observed for 1 and 2 wt % GO composites, the sheets protruding from the surface appeared to be many layers thick (in accordance with TEM observations). High aspect ratio voids in the surface, or "pull-out" voids, where GO sheets were pulled from the material during fracture were observed in the GO nanocomposite materials. This observation, along with the relatively "uncoated" nature of the GO sheets suggests that the interaction between the cyanate ester matrix and the GO sheets is predominantly noncovalent. The GO particles, however, remain well-dispersed during cure, that is, no significant phase separation took place. This inference is supported by the observation that the composite GO samples were clear dark green in color while the TRGO and M-25 composites were opaque and black.

In contrast, SEM images of TRGO composite samples show a markedly different surface texture compared to the GO composites (Fig. 6). Phase separation was apparent in the SEMs of the fractured surface of TRGO and was readily apparent in low magnification SEMs (see Supporting Information). The sharpness of TRGO composite micrographs was reduced somewhat due to the high contrast in conductivity between TRGO (relatively conductive) and LECy (an insulator). Thus, the TRGO rich regions dissipate charge readily while charge dissipation is absent in the surrounding LECy matrix, leading to high contrast in the SEM images. The TRGO nanocomposites thus show evidence of phase separation on the scale of tens of microns, and the formation of a percolating network of TRGO-rich regions.

The direct incorporation of untreated M-25 GNP into the LECy resulted in very poor dispersion, with composite

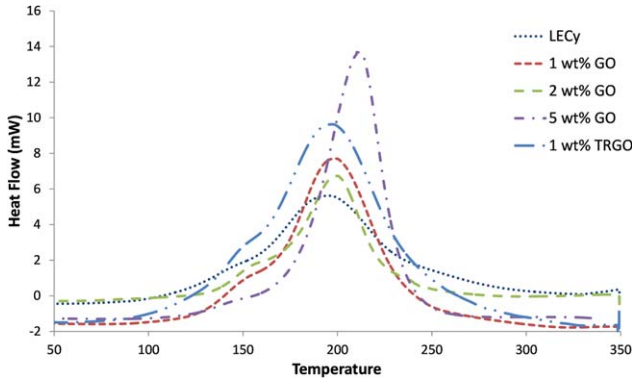

FIGURE 7 Dynamic Differential Scanning Calorimetry (DSC) of catalyzed LECy and catalyzed LECy/GO mixtures. [Color figure can be viewed in the online issue, which is available at wileyonlinelibrary.com.]

specimens showing large voids. Although cyanate esters are typically described as "medium polarity" resins, the highly polar GO showed the best compatibility characteristics, while the relatively nonpolar TRGO showed limited compatibility. The likely least polar M-25 GNP showed essentially no compatibility. In the case of TRGO, the "shredded sheet" nanoscale morphology in which sheets appear to be mechanically linked to some extent may have played an important role in preventing full dispersion. With respect to polarity, therefore, we can only conclude that the highly polar GO retains good compatibility with the cyanate ester matrix, because good micron-scale dispersion was achieved without any apparent covalent bonding, while the nonpolar M-25 GNP surfaces showed little or no compatability with the cyanate ester matrix.

Properties of Graphene and LECy-Graphene Composites

Having established the effects of oxidation and subsequent thermal reduction of graphene on the resultant morphology of cyanate ester nanocomposites, the relationship between nanocomposite structure and properties can be better understood. In this section, we focus primarily on GO and TRGO nanocomposites, as the M-25 GNP/polycyanurate systems are of limited usefulness due to poor dispersion of the graphene. A first key consideration to be investigated was whether the presence of any form of graphene significantly altered either the cure kinetics or the resulting chemical structure of the cyanate ester matrix. Dynamic DSC showed that the addition of either GO or TRGO resulted in only a modest downward shift in peak exotherm temperatures, and no significant reduction in the processing window of the liquid monomer LECy (Fig. 7). It has been observed that GO decreases the peak temperature of the cure exotherm in uncatalyzed PT-30 polycyanurate thereby narrowing the processing window.[33] However, the LECy mixtures in this study included both a phenolic catalyst and a copper accelerator. The presence of hydroxylated graphene surfaces at the loading levels examined does not appear to add significantly to the already substantial catalysis of the system. Thus, in strongly catalyzed cyanate esters, the presence of graphene is unlikely to compromise the technologically important advantage of the wide processing window associated with LECy.

TABLE 2 Fracture Toughness of 1 wt % GO and TRGO LECy Composites

Sample	K_q (MPa $m^{1/2}$)
LECy	1.07 ± 0.34
1 wt % GO	1.49 ± 0.08
1 wt % TRGO	1.40 ± 0.23

FTIR of neat LECy, GO, and TRGO nanocomposites confirms that conversion of cyanate ester groups to triazine rings, typical of cyanate cure, is the dominant reaction in the presence of GO and TRGO (see Supporting Information). This data demonstrates that the addition of either GO or TRGO does not alter the network matrix through reactions with either functional groups at the surface or impurities associated with the chemical oxidation of graphite to produce GO.

The presence of both GO and TRGO resulted in an increase in fracture toughness over neat LECy (Table 2). The type of graphene, oxidized, or thermally reduced, did not have a significant effect on the magnitude of fracture toughness improvement over pure LECy. However, the mechanism of fracture toughness improvement may be different with each form of graphene. In the case of GO, the high degree of oxidation allows for good dispersion of GO particles and therefore increased toughness. However, TRGO was not dispersed as well as GO but exists as a phase separated and percolated network of disordered sheets that results in increased toughness.

The incorporation of GO in LECy polycyanurate resulted in an increased storage modulus as measured by DMA at loadings up to 2 wt % (Fig. 8). Further addition of GO resulted in a decrease in storage modulus, resulting in a value

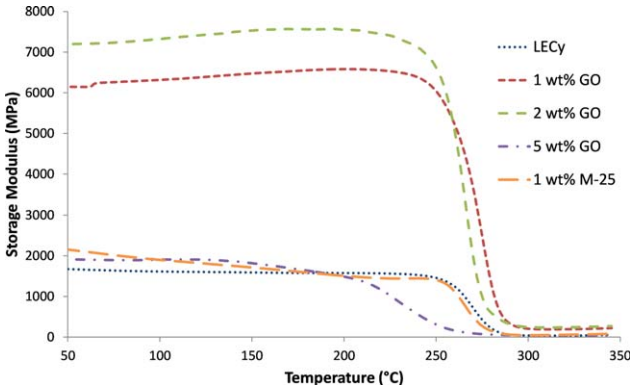

FIGURE 8 Storage moduli of 1, 2, and 5 wt % GO composites and 1 wt % M-25 obtained by DMA. [Color figure can be viewed in the online issue, which is available at wileyonlinelibrary.com.]

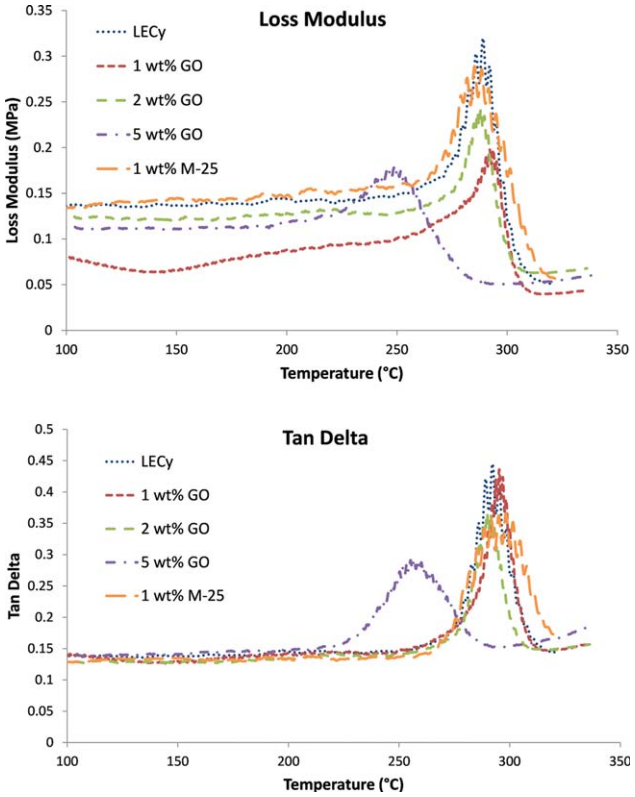

FIGURE 9 Loss Modulus and Tan Delta of GO and M-25 graphite composites obtained by Thermomechanical Analysis (TMA). [Color figure can be viewed in the online issue, which is available at wileyonlinelibrary.com.]

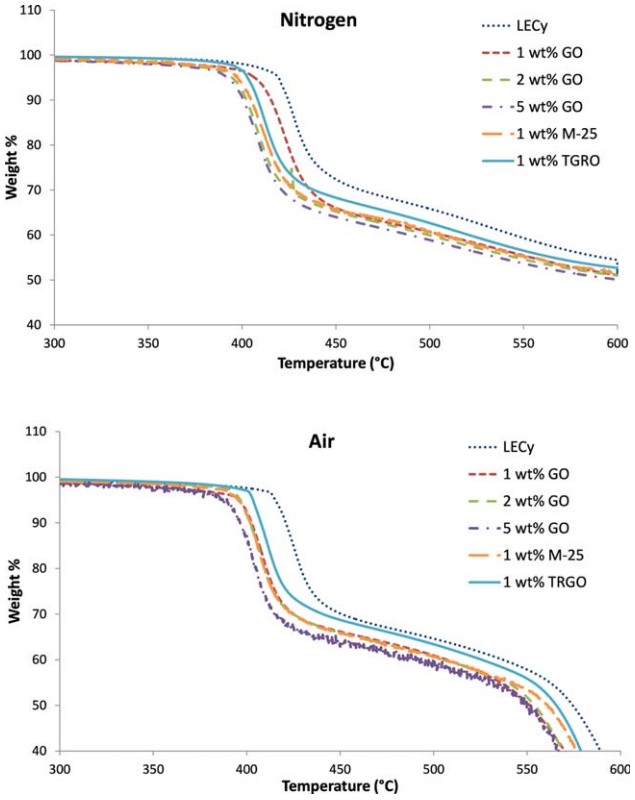

FIGURE 10 Thermogravimetric analysis (TGA) of GO, M-25 graphite and TRGO composites. [Color figure can be viewed in the online issue, which is available at wileyonlinelibrary.com.]

close to that of the neat resin. It should be noted that the storage moduli values in Figure 8 represent the properties of fully cured samples, since these materials underwent some post cure in the DMA instrument. The thermomechanical behavior of as-cured materials is available in Supporting Information. The addition of 1% M-25 GNP, which resulted in poor dispersion, as noted earlier, produced essentially no change in storage modulus. Well-dispersed GO at low loadings in the LECy matrix increased relative stiffness through favorable noncovalent interactions between GO and the polycyanurate matrix. However, poor dispersion of the M-25 graphite due to the absence of surface functionalities that lead to favorable interactions resulted in no reinforcing effect.

TABLE 3 CTE at 75 °C, Loss Modulus, and Tan Delta Peak Temperatures of GO and TRGO Composites Obtained by TMA

Sample	CTE (ppm °C^{-1})	Fully Cured Loss Modulus Peak (°C)	Fully Cured Tan Delta Peak (°C)
LECy	50 ± 1	289 ± 9	292 ± 9
1 wt % GO	57	294	295
2 wt % GO	52	288	290
5 wt % GO	50	250	257
1 wt % M-25	50	288	298

The addition of neither GO nor M-25 affected the glass transition temperatures of the corresponding fully cured composites (Fig. 9, Table 3) with the exception of 5% GO, which showed bubble formation during cure (see Supporting Information). As with DMA, all of the composite materials displayed an identical T_g by TMA to that of neat LECy, with the exception of 5 wt % GO, which showed a T_g ~40 °C lower than the other materials. The CTE (also shown in Table 3) was highest for the 1 wt % GO composite followed by the 2 wt % GO composite, while both exhibited CTE values only modestly greater than neat LECy. All of these results indicate that at low loading, where the release of gases due to heating of the GO can be accommodated without damaging the matrix, the presence of GO has minimal effects on the thermo-mechanical performance of the network.

To examine the effect of the degree of graphene oxidation on nanocomposite thermo-chemical stability, TGA was performed in nitrogen and air on the cured nanocomposite specimens. All of the nanocomposite materials displayed a lower 5 and 10 wt % loss temperature than LECy (Fig. 10), with the 5 wt % GO composite displaying the lowest weight loss temperatures in both nitrogen and air (Table 4). Greater amounts of GO content generally resulted in lower 5 and 10 wt % loss temperatures. The composite with 1 wt % TRGO displayed slightly higher weight loss temperatures than the

TABLE 4 Weight Loss Temperatures and Char Yields of GO, Thermally Reduced GO, and M-25 Graphite Composites in Nitrogen and Air

		Nitrogen			Air	
Sample	5 % Weight Loss (°C)	10 % Weight Loss (°C)	Char Yield at 600 °C (%)	5 % Weight Loss (°C)	10 % Weight Loss (°C)	Char Yield at 600 °C (%)
LECy	419 ± 3	424 ± 2	54 ± 1	415 ± 8	421 ± 9	32 ± 3
1 wt % GO	405	415	51	394	402	20
2 wt % GO	393	402	51	396	401	13
5 wt % GO	390	400	50	386	396	13
1 wt % M-25	396	404	52	394	402	19
1 wt % TRGO	402	408	53	403	407	19

1 wt % GO composite in air, while lower weight loss temperatures were observed in nitrogen. Char yields of the composites were lower than pure LECy in air while remaining approximately the same as LECy in nitrogen. Improved thermal stability has been observed for PS, PVA and PMMA composites with graphene; however, the improved thermal stability of these materials was attributed to restriction of mobility of polymer segments through favorable interactions, both covalent and noncovalent, between graphene and the polymer matrix.[8,16,39] In contrast, the segmental polymer chain mobility of the polycyanurate-graphene polymer systems in this study appear unaffected by the presence of graphene as evidenced by the constant T_g of these systems. Introduction of surface functional groups on graphene results in decreased thermal stability of the corresponding nanocomposite. This effect is not surprising given that these groups are less thermodynamically stable than pristine graphene and given the thermal lability of the oxygen moieties on GO. Fortunately, due to the low loading levels of graphene present, the reductions in thermo-chemical stability remain modest, and graphene/cyanate ester nanocomposites maintain much of the desirable improvement in thermochemical stability of polycyanurates compared to other thermosetting resins.

Despite the reportedly good barrier properties of graphene-based reinforcements, the presence of GO and TRGO at 1 wt % did not affect the D of water in LECy (Table 5). In fact, equilibrium water uptake for both composites was higher than the neat polycyanurate (Fig. 11). This result suggests that, even if the addition of some forms of graphene creates a more tortuous pathway for water to diffuse into the material, nonbonded regions, microvoids, and/or sites preferential to water uptake may be created at the polymer matrix interface for both GO and TRGO composites. It is not surprising that the addition of GO, which contains functionalities that hydrogen bond with water, results in a higher equilibrium water uptake. The equilibrium water uptake of GO composites suggests that water may be residing in void spaces between graphene layers and the polycyanurate matrix. Furthermore, GO in these composites is not fully exfoliated, as seen in TEM, and the interlaminar space between GO sheets is known to be a favorable site for water to reside. In fact, GO films are excellent barriers for many organic solvents, and gasses but allow unimpeded permeation of water.[40] Although the presence of isolated, highly anisotropic GO platelets might be expected to result in a more tortuous pathway for water diffusion, the stacked morphology of the GO simultaneously provides a "super highway" for the unimpeded permeation of water through each isolated platelet, eliminating the expected tortuosity effect and thereby resulting in no net change in water diffusion with respect to neat LECy polycyanurate.

It is somewhat surprising that the degree of oxidation, and therefore the amount of hydrophilic functional groups, of the nano-reinforcement did not affect the D or equilibrium water

TABLE 5 Equilibrium Water Uptake and D of LECy, GO, and TRGO Composites

Sample	M_m (%)	$D{\cdot}10^{-8}$ (cm^2 s^{-1})
LECy	1.1	1.2
1 wt % GO	1.8	1.1
1 wt % TRGO	1.7	1.2

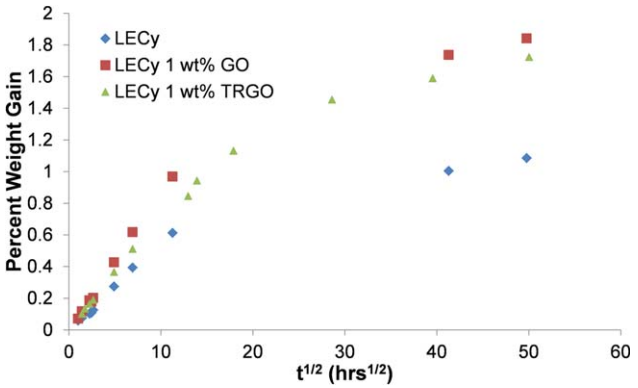

FIGURE 11 Ambient temperature water uptake of LECy, 1 wt % GO, and 1 wt % TRGO. [Color figure can be viewed in the online issue, which is available at wileyonlinelibrary.com.]

uptake as can be seen by the identical equilibrium weight gain and *D* for the GO and TRGO composites. The addition of TRGO to an epoxy matrix at only 0.1 wt % decreased the equilibrium water uptake to half of that of the pure epoxy resin.[22] The epoxy matrix, however, has a relatively high equilibrium water uptake (~5 wt %) when compared with LECy polycyanurate. Therefore, the effects of a material that influences water uptake may be more apparent with an epoxy matrix than a relatively low water absorption medium such as polycyanurate. Moreover, thermal treatment of GO to produce TRGO results in increased disorder, as can be seen by the "shredded" nanoscale morphology of TRGO in TEM, which is expected to be less effective at reducing diffusion and results in increased percolation, observed as phase separation in SEM. Therefore, the presence of a percolated reinforcement with a nonbonded interface may provide pathways for water diffusion that, although potentially more tortuous, are generally of lower resistance and lead to increased equilibrium water uptake.

To achieve decreased water permeation in graphene-based polycyanurate nanocomposites, it appears that one needs both good dispersion of particles and a low concentration of polar groups at the surface. As mentioned earlier, however, there appears to be a trade-off between particle/matrix compatibility and surface polarity, such that attaining both of the needed characteristics for lowering the permeation of cyanate ester composites is not readily achieved. The incorporation of graphene-based reinforcements with a well-bonded interface, in which compatibility is enhanced by chemical grafting, may overcome this obstacle to achieving reduced water permeation.

CONCLUSIONS

A comparative study of the reinforcement of polycyanurate networks with three forms of graphene, edge-functional nanoplatelets (GNP), GO derived from these nanoplatelets (GO), and thermally reduced GO (TRGO) derived from the aforementioned GO, showed a significant trade-off between compatibility and the level of functionalization. GNP showed virtually no dispersibility, GO showed good dispersion even after cure, but individual particles consisted of non-exfoliated layer stacks with some intercalated water. TRGO showed more limited dispersion, forming percolated particle networks with little or no intercalated water. In the case of TRGO, a significant alteration in the nanoscale morphology of the graphene induced by thermal treatment (that is, the formation of "shredded" stacks) likely played a significant role in limiting the dispersibility. The addition of both GO and TRGO to LECy polycyanurate resulted in improved stiffness and fracture toughness at low loading levels without sacrificing the wide processing window of cyanate ester resins or altering the chemistry of network formation.

Somewhat surprisingly, however, no reduction in the *D* of water was achieved with the incorporation of either GO or TRGO, while a greater equilibrium water uptake was observed in nanocomposites containing both forms of graphene. In the case of GO, the water-intercalated structure is believed to have provided a "shortcut" for permeation through the plate-like particles, eliminating the need for water to follow a tortuous path through the nanocomposites. In the case of TRGO, the formation of percolated particle networks may have induced a similar effect. In both cases, the presence of a nonbonded interface with a high specific surface area may have provided more sites for water sorption. The results for cyanate esters were significantly different than for epoxy resins, pointing to the need to carefully consider the specific morphologies and particle-matrix interactions in graphene nanocomposites when considering the effects of graphene reinforcement on physical properties.

ACKNOWLEDGMENTS

This research was performed while JTR held a National Research Council Research Associateship Award at the Air Force Research Laboratory (AFRL). The authors gratefully acknowledge the Air Force Office of Scientific Research and the AFRL, Rocket Propulsion Division for their financial support. Thanks to Sean Ramirez at AFRL for assistance with XRD data and Barbara Miller at AFRL/UDRI for performing TEM imaging.

REFERENCES AND NOTES

1 C. Lee, X. D. Wei, J. W. Kysar, J. Hone, *Science* **2008**, *321*, 385–388.

2 A. A. Balandin, S. Ghosh, W. Z. Bao, I. Calizo, D. Teweldebrhan, F. Miao, C. N. Lau, *Nano Lett.* **2008**, *8*, 902–907.

3 X. Du, I. Skachko, A. Barker, E. Y. Andrei, *Nat. Nanotechnol.* **2008**, *3*, 491–495.

4 J. S. Bunch, S. S. Verbridge, J. S. Alden, A. M. van der Zande, J. M. Parpia, H. G. Craighead, P. L. McEuen, *Nano Lett.* **2008**, *8*, 2458–2462.

5 K. S. Novoselov, A. K. Geim, S. V. Morozov, D. Jiang, Y. Zhang, S. V. Dubonos, I. V. Grigorieva, A. A. Firsov, *Science* **2004**, *306*, 666–669.

6 O. Leenaerts, B. Partoens, F. M. Peeters, *Appl. Phys. Lett.* **2008**, *93*, 193107.

7 A. B. Bourlinos, V. Georgakilas, R. Zboril, T. A. Steriotis, A. K. Stubos, *Small* **2009**, *5*, 1841–1845.

8 N. Liu, F. Luo, H. X. Wu, Y. H. Liu, C. Zhang, J. Chen, *Adv Funct Mater* **2008**, *18*, 1518–1525.

9 Y. Hernandez, V. Nicolosi, M. Lotya, F. M. Blighe, Z. Y. Sun, S. De, I. T. McGovern, B. Holland, M. Byrne, Y. K. Gun'ko, J. J. Boland, P. Niraj, G. Duesberg, S. Krishnamurthy, R. Goodhue, J. Hutchison, V. Scardaci, A. C. Ferrari, J. N. Coleman, *Nat. Nanotechnol.* **2008**, *3*, 563–568.

10 N. Behabtu, J. R. Lomeda, M. J. Green, A. L. Higginbotham, A. Sinitskii, D. V. Kosynkin, D. Tsentalovich, A. N. G. Parra-Vasquez, J. Schmidt, E. Kesselman, Y. Cohen, Y. Talmon, J. M. Tour, M. Pasquali, *Nat. Nanotechnol.* **2010**, *5*, 406–411.

11 B. C. Brodie, *Philos Trans R Soc London* **1859**, *149*, 249–259.

12 L. Staudenmaier, *Ber. Dtsch. Chem. Ges.* **1898**, *31*, 1481–1487.

13 W. S. Hummers, R. E. Offeman, *J. Am. Chem. Soc.* **1958**, *80*, 1339–1339.

14 A. Lerf, H. Y. He, M. Forster, J. Klinowski, *J. Phys. Chem. B* **1998**, *102*, 4477–4482.

15 H. Y. He, J. Klinowski, M. Forster, A. Lerf, *Chem. Phys. Lett.* **1998**, *287*, 53–56.

16 J. I. Paredes, S. Villar-Rodil, A. Martinez-Alonso, J. M. D. Tascon, *Langmuir* **2008**, *24*, 10560–10564.

17 H. Kim, A. A. Abdala, C. W. Macosko, *Macromolecules* **2010**, *43*, 6515–6530.

18 M. J. McAllister, J. L. Li, D. H. Adamson, H. C. Schniepp, A. A. Abdala, J. Liu, M. Herrera-Alonso, D. L. Milius, R. Car, R. K. Prud'homme, I. A. Aksay, *Chem. Mater.* **2007**, *19*, 4396–4404.

19 H. C. Schniepp, J. L. Li, M. J. McAllister, H. Sai, M. Herrera-Alonso, D. H. Adamson, R. K. Prud'homme, R. Car, D. A. Saville, I. A. Aksay, *J. Phys. Chem. B* **2006**, *110*, 8535–8539.

20 V. Singh, D. Joung, L. Zhai, S. Das, S. I. Khondaker, S. Seal, *Prog. Mater. Sci.* **2011**, *56*, 1178–1271.

21 M. A. Rafiee, J. Rafiee, Z. Wang, H. H. Song, Z. Z. Yu, *Acs Nano* **2009**, *3*, 3884–3890.

22 O. Starkova, S. Chandrasekaran, L. Prado, F. Tolle, R. Mulhaupt, K. Schulte, *Polym. Degrad. Stabil.* **2013**, *98*, 519–526.

23 D. R. Bortz, E. G. Heras, I. Martin-Gullon, *Macromolecules* **2012**, *45*, 238–245.

24 M. A. Rafiee, J. Rafiee, I. Srivastava, Z. Wang, H. H. Song, Z. Z. Yu, N. Koratkar, *Small* **2010**, *6*, 179–183.

25 M. Fang, Z. Zhang, J. F. Li, H. D. Zhang, H. B. Lu, Y. L. Yang, *J. Mater. Chem.* **2010**, *20*, 9635–9643.

26 I. Hamerton, Chemistry; Technology of Cyanate Ester Resins; Chapman & Hall: London, UK, **1994**.

27 B. Yameen, H. Duran, A. Best, U. Jonas, M. Steinhart, W. Knoll, *Macromol. Chem. Phys.* **2008**, *209*, 1673–1685.

28 A. J. Guenthner, G. R. Yandek, J. M. Mabry, K. R. Lamison, V. Vij, M. C. Davis, L. R. Cambrea, Proceedings of SAMPE '10, Vol. 55; SAMPE In-ternational Business Office: Covina, CA, **2010**; paper 42ISTC-119.

29 A. J. Guenthner, K. R. Lamison, G. R. Yandek, K. C. Masurat, J. T. Reams, L. R. Cambrea, J. M. Mabry, *Polym. Preprints* **2011**, 52.

30 X. Sheng, R. Hanus, A. Bauer, M. R. Kessler, *J. Appl. Polym. Sci.* **2013**, *130*, 463–469.

31 P. Badrinarayanan, J. Leonard, M. R. Kessler, *J. Nanosci. Nanotechnol.* **2011**, *11*, 3970–3978.

32 Q. L. Lin, L. J. Qu, Q. F. Lu, C. Q. Fang, *Polym. Test* **2013**, *32*, 330–337.

33 X. Wang, J. Jin, M. Song, *Eur. Polym. J.* **2012**, *48*, 1034–1041.

34 L. N. Britton, R. B. Ashman, T. M. Aminabhavi, P. E. Cassidy, *J. Chem. Edu.* **1988**, *65*, 368–370.

35 J. Comyn, B. C. Cope, M. R. Werrett, *Polym. Commun.* **1985**, *26*, 294–296.

36 T. Szabo, O. Berkesi, P. Forgo, K. Josepovits, Y. Sanakis, D. Petridis, I. Dekany, *Chem. Mater.* **2006**, *18*, 2740–2749.

37 M. Fang, K. G. Wang, H. B. Lu, Y. L. Yang, S. Nutt, *J. Mater. Chem.* **2009**, *19*, 7098–7105.

38 H. D. Huang, P. G. Ren, J. Chen, W. Q. Zhang, X. Ji, Z. M. Li, *J. Membr. Sci.* **2012**, *409*, 156–163.

39 H. J. Salavagione, M. A. Gomez, G. Martinez, *Macromolecules* **2009**, *42*, 6331–6334.

40 R. R. Nair, H. A. Wu, P. N. Jayaram, I. V. Grigorieva, A. K. Geim, *Science* **2012**, *335*, 442–444.